Journal of Glaciology

Letter

Cite this article: Sunako S, Fujita K, Izumi T, Yamaguchi S, Sakai A, Kayastha RB (2023). Up-glacier propagation of surface lowering of Yala Glacier, Langtang Valley, Nepal Himalaya. *Journal of Glaciology* **69**(274), 425–432. https://doi.org/10.1017/jog.2022.118

Received: 13 October 2021
Revised: 6 October 2022
Accepted: 1 November 2022
First published online: 24 January 2023

Keywords:
Glacier mass balance; glacier monitoring; mountain glaciers

Author for correspondence:
Sojiro Sunako,
E-mail: s_sunako667@bosai.go.jp

cambridge.org/jog

Up-glacier propagation of surface lowering of Yala Glacier, Langtang Valley, Nepal Himalaya

Sojiro Sunako[1], Koji Fujita[2], Takeki Izumi[3], Satoru Yamaguchi[1], Akiko Sakai[2] and Rijan Bhakta Kayastha[4]

[1]Snow and Ice Research Center, National Research Institute for Earth Science and Disaster Resilience (NIED), Nagaoka, Japan; [2]Graduate School of Environmental Studies, Nagoya University, Nagoya, Japan; [3]Graduate School of Urban Environmental Sciences, Tokyo Metropolitan University, Hachioji, Japan and [4]Department of Environmental Science and Engineering, Himalayan Cryosphere, Climate and Disaster Research Center (HiCCDRC), School of Science, Kathmandu University, Dhulikhel, Nepal

Abstract

We quantify the surface elevation changes along Yala Glacier in Langtang Valley, Nepal Himalaya, since 1981 using geodetic methods to understand the recent evolution and current state of small debris-free glaciers across the region. We analyse differential global positioning system measurements and aerial stereo imagery that were acquired along Yala Glacier in 2007, 2009, 2012 and 2015 to generate digital elevation models for each calculation period. Continuous surface lowering has mainly been observed across the down-glacier area during the calculation periods, although a large degree of variability exists, with this lowering trend propagating up-glacier in recent years. The area-weighted glacier mass balances range from -0.98 ± 0.27 to -0.26 ± 0.30 m w.e. a^{-1} for the five calculation periods (1981–2007, 2007–2009, 2009–2012, 2012–2015 and 2007–2015). These calculated mass-balance data reveal that Yala Glacier has undergone accelerated mass loss since the late 2000s, which is consistent with the results of previous in situ measurement and remote-sensing studies.

Introduction

Glacier-monitoring studies in High Mountain Asia are vital for understanding their complex degree of mass-balance fluctuations due to recent climatic conditions (e.g. Azam and others, 2018; Maurer and others, 2019). Studies using satellite-based digital elevation models (DEMs) have revealed continuous mass loss across the Himalaya, with the exceptions of the Karakoram and Kunlun mountain ranges, where slight mass losses or even gains have been observed (e.g. Brun and others, 2017; Shean and others, 2020). Ground-based mass-balance observations across various Himalayan glaciers are therefore critical for ground truthing since the combination of individual valley climates and glacier characteristics has resulted in heterogeneous mass changes, even within the same region (e.g. Ragettli and others, 2016; Vijay and Braun, 2016; King and others, 2017). However, in situ observational studies remain scarce due to the remoteness of these glaciers and the associated logistical difficulties (e.g. Yao and others, 2012; Azam and others, 2016; Sherpa and others, 2017; Sunako and others, 2019; Angchuk and others, 2021; Stumm and others, 2021). Previous studies have employed global positioning system (GPS) and/or rangefinders during repeated surveys to derive point-based DEMs and capture surface elevation changes, and therefore estimate geodetic glacier mass balances (e.g. Fujita and Nuimura, 2011; Tshering and Fujita, 2016). Precise GPS positions have also been used to validate satellite-based DEMs (e.g. Fujita and others, 2008; Nuimura and others, 2012; Berthier and others, 2014; Wagnon and others, 2021). Furthermore, recent studies have employed uncrewed aerial vehicles (UAVs) and applied the Structure from Motion technique (SfM) to generate high-precision DEMs for glaciological monitoring, thereby allowing for detailed analyses of the morphological changes along the glacier surface (e.g. Immerzeel and others, 2014; Kraaijenbrink and others, 2016; Vincent and others, 2016; Brun and others, 2018; Sato and others, 2021; Mishra and others, 2021). However, these UAV-based studies have mainly been limited to debris-covered glaciers owing to the extreme atmospheric conditions in the high-elevation Himalaya. Here we report on surface elevation changes and geodetic mass balances of a small debris-free glacier in the Nepal Himalaya for a series of time intervals during the 1981–2015 period using digitised map-, GPS-, airborne- and UAV-derived DEMs.

Study site, data and methodology

Study site

The debris-free Yala Glacier (RGI60-15.03954; 28.236°N, 85.617°E) is located along Langtang Valley in the central Nepal Himalaya. Langtang Valley contains a glacierised area of approximately 120 km^2, with Yala Glacier covering 1.54 km^2 in 2015 (Figs. 1a and b). The elevation of the glacier ranges from approximately 5140 to 5690 m above sea level (a.s.l.), and it flows to the southwest, with a mean surface slope of 25°. Yala Glacier is one of the benchmarks in the Nepal Himalaya, as in situ glaciological and geodetic mass-balance measurements have been

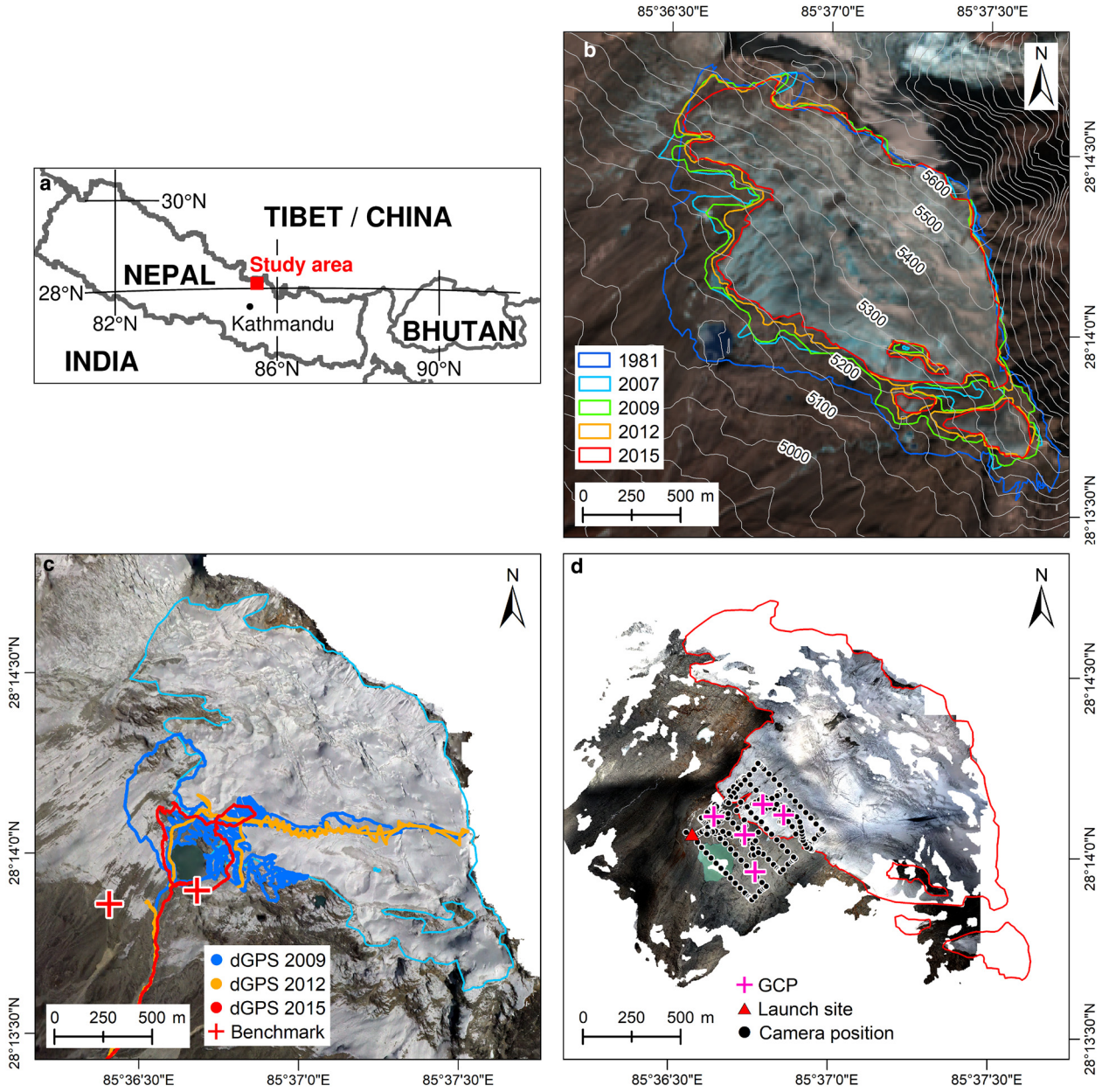

Fig. 1. (a) Regional map, showing the location of the study area (Langtang valley, red box) and Kathmandu, the capital city of Nepal. (b) Map of Yala Glacier and its boundaries in 1981, 2007, 2009, 2012 and 2015 (blue, light-blue, green, orange and red polygons, respectively). (c) Ortho image of Yala Glacier, which was generated from the 2007 aerial photogrammetry survey, with the 2009, 2012 and 2015 dGPS tracks (blue, orange and red circles, respectively) and benchmarks (red crosses) indicated. (d) Ortho image of Yala Glacier derived from the 2015 UAV photogrammetry survey, with the UAV launch site (red triangle), ground control points (GCPs, pink crosses) and camera positions (black circles) indicated. Contour lines in (b) are derived from the ALOS World 3D (30 m resolution), and the background image is a Sentinal-2 composite image that was acquired on 28 December 2015.

acquired intermittently since 1982 (Ageta and others, 1984). Several studies have revealed that the glacier has been in a state of negative mass balance in recent decades (e.g. Fujita and Nuimura, 2011; Sugiyama and others, 2013). Acharya and Kayastha (2019) conducted in situ mass balance measurements for the 2011–2017 period, and Stumm and others (2021) updated a mass loss value of -0.80 ± 0.28 m water equivalent (w.e.) a^{-1}, with a mean equilibrium line altitude of 5456 m a.s.l. for the same study period. Shean and others (2020) reported a mass loss of -0.78 ± 0.13 m w.e. a^{-1} for the 2000–2018 period from remote-sensing observations.

Differential GPS survey

In situ measurements were acquired in October 2009, May 2012 and October 2015 (Table 1). We conducted differential GPS (dGPS) surveys (GEM-1 and 2, Enabler, Inc.; and R10, Nikon-Trimble Co., Ltd.) during each measurement period. A GPS base station was installed at Kyangjin Village (28.212°N, 85.565°E; 5.5 km from Yala Glacier), with other GPS receivers roving in kinematic mode at a 1-s recording interval. The uncertainty in the dGPS systems was reported to be ~0.2 m in previous studies (e.g. Fujita and others, 2008; Vincent and others, 2016). We established two benchmarks around the glacier (Fig. 1c). The 2009 GPS data have been evaluated by Fujita and Nuimura (2011) and Sugiyama and others (2013); here we reanalysed this dataset using our 2012 measurement. The obtained GPS records were post-processed using the RTKLIB software (http://www.rtklib.com/, last accessed on 20 May 2020) and projected onto the Universal Transverse Mercator coordinate system (zone 45N, WGS-84 reference system) as elevations above the ellipsoid (m; hereafter, elevations). The exact location of the base station

https://doi.org/10.1017/jog.2022.118 Published online by Cambridge University Press

Table 1. Acquisition and resolution details of the digital elevation models employed for the elevation change calculations in this study

Name	Date	Resolution (m)	Method obtained	Source	Shift easting (m)	Shift northing (m)	Mean[a] (m)	SD[b] (m)	NMAD[a] (m)
MAP-DEM	24 Nov 1981	10	Digitised map	Yokoyama (1984); Fujita and Nuimura (2011)	20.00	−10.00	111.80	4.58 (5.27)	4.37
The 2007 DEM	2 Dec 2007	2	Oblique aerial photogrammetry	This study	0.00	−4.00	0.09	1.41 (1.70)	1.39
		10			0.00	0.00	−0.17	1.41 (1.75)	1.41
The 2009 GPS-DEM	30 Oct–3 Nov 2009	1	dGPS measurements	Fujita and Nuimura (2011)	0.00	−1.00	0.40	0.14 (1.41)	0.20
		2			0.00	0.00	0.32	0.33 (0.88)	0.32
The 2012 GPS-DEM	5–8 May 2012	1	dGPS measurements	This study	0.00	−1.00	0.49	0.11 (0.26)	0.10
UAV-DEM	28 Oct 2015	1	UAV-based photogrammetry	This study	0.00	0.00	0.04	0.23 (0.40)	0.23
		2			0.00	0.00	0.06	0.28 (0.43)	0.31

The 2015 GPS-DEM, which was acquired on 28 October 2015, is used as a reference DEM. The horizontal shifts of each DEM (easting and northing), and the mean, std dev. (SD) and normalised median absolute deviation (NMAD) of the elevation differences between each DEM and the 2015 GPS-DEM are provided. The SD values before co-registration are given in brackets.
[a]After horizontal co-registration.
[b]After horizontal co-registration and detrending function applied.

was determined via the Precise Point Positioning service operated by Natural Resources Canada (https://webapp.geod.nrcan.gc.ca/geod/tools-outils/ppp.php, last accessed on 20 May 2020), with the exception of the 2009 GPS records, when a single-frequency dGPS system was employed. The 2009 GPS-DEM was co-registered against the 2012 GPS-DEM using the benchmark locations. We then generated 1 m DEMs for 2009, 2012 and 2015 by applying the inverse distance weighted interpolation function in the ArcGIS Pro software to the dGPS data and employing a search radius of $x/\sqrt{2}$ (in m), where x is the resolution, based on Fujita and others (2017). The grid cells with no dGPS points were systematically removed, following Tshering and Fujita (2016). The 2015 GPS-DEM was additionally resampled to 2, 8 and 10 m resolutions for comparison with the other DEMs employed in this study.

Aerial photogrammetry

A UAV-based photogrammetric survey, which was a component of the Gorkha earthquake-induced disaster investigation in Langtang Valley (Fujita and others, 2017), was conducted on 28 October 2015. A PD6-NPL hexacopter (PRODRONE Co. Ltd., Nagoya, Japan; Fig. S1), which is capable of ∼15 min-duration flights, was employed for the survey. The hexacopter was equipped with a full-frame mirrorless camera (Sony α7R) that had a 36.4 megapixel sensor size (7360 by 4912 pixels) and interchangeable lens (28 mm focal length). Two flights were flown in manual mode at a mean flying altitude of ∼230 m above the ground-surface, with the lines limited largely to the glacier terminus (Fig. 1d). We therefore acquired photographs of the upper part of the glacier by changing the camera angles. We placed five orange fabric sheets (1 × 1 m) at on/off-glacier areas the day before the UAV flights to obtain ground control points (GCPs). The precise GCP positions were measured via dGPS at a 1-min interval based on a similar methodology to that in previous studies (Immerzeel and others, 2014; Fujita and others, 2017).

We further analysed 14 oblique aerial photographs that were acquired by a private jet with two handheld cameras (Canon EOS 5D and Canon EOS-1Ds Mark2) in December 2007 to generate an ortho image and DEM. Although the exact flight height was not recorded during this flight, the mean flying altitude was estimated to be ∼6700 m based on a nearby study at a similar glacier altitude that employed the same private jet (Sato and others, 2021). We extracted 32 GCPs from specific features on the off-glacier terrain of the 2017 Pléiades-DEM and the ortho image for the 2007 dataset (Fig. S2) based on the method proposed by Sato and others (2021). The Pléiades-DEM was both horizontally and vertically shifted to the 2015 GPS-DEM based on the method of Nuimura and others (2012) and Rolstad and others (2009) (see the 'Bias calibration' section).

Map and satellite data

We derived the 1981 DEM from a map that was generated using ground photogrammetry images that were acquired in November 1981 (Yokoyama, 1984) to calculate the elevation changes. Fujita and Nuimura (2011) subsequently digitised the 1981 map and interpolated it to a 10 m resolution (Fujita and Nuimura, 2011; hereafter, MAP-DEM). We re-georeferenced the digitised map and DEM to align with the key features that were detected in a Landsat image acquired in October 1988.

We further utilised the High Mountain Asia 8 m DEM (Shean, 2017; hereafter, HMA-DEM), which was derived on 29 December 2015, to obtain the 2015 hypsometry. We also used Landsat and Advanced Spaceborne Thermal Emission and Reflection Radiometer (ASTER) images to delineate the glacier area. The satellite data used in this study are listed in Table S1.

DEM generation

SfM software (Agisoft Metashape Professional Version 1.6.0) was utilised to generate the 2007 and 2015 DEMs and ortho images following the standard SfM processing workflow (Lucieer and others, 2014; Agisoft, 2020). The key details of the cameras and the SfM processing parameters are listed in Table S2. We processed 14 and 519 images in 2007 and 2015 to generate sparse point clouds with ultrahigh- and high-quality settings, respectively. We manually added GCPs to georeference the point clouds, and produced dense point clouds. We employed the 'dense cloud confidence' parameter, which is the number of images referenced for generating dense point clouds, to remove any outliers whose values were <2. The generated DEMs were resampled to 2 m (2007) and 1 m (2015), and the original resolution of the ortho image was exported for comparison (Table S2).

Glacier outlines

The glacier boundaries were delineated from the digitised 1981 map, 2007 aerial photogrammetry-derived ortho image, and visible or panchromatic Landsat Thematic Mapper (TM; 30 m resolution), ASTER (15 m resolution) and Landsat Operational Land Imager (OLI; 15 m resolution) bands, which were acquired in 2009, 2012 and 2015, respectively (Fig. 1b; Table S1). We excluded the DEM grids in the buffer zones along the glacier boundaries, which were defined as ±1 pixel zones in the referenced images, to clearly distinguish the on- and off-glacier areas.

https://doi.org/10.1017/jog.2022.118 Published online by Cambridge University Press

Bias calibration

The DEMs used to calculate elevation changes are listed in Table 1. We first shifted all of the DEMs, including the Pléiades-DEM and HMA-DEM, horizontally (into both the easting and northing directions) to minimise the std dev. of the elevation changes between these DEMs and the 2015 GPS-DEM over the stable terrain (<30° slope) of the off-glacier area along the dGPS tracks (Nuimura and others, 2012). We then calculated the normalised median absolute deviation (NMAD) across the off-glacier area, excluded the calculated values that were greater than ±3 NMAD from the mean values as outliers (Höhle and Höhle, 2009). We further determined a first-order (linear) detrending function using a least-squares fit between each DEM and the 2015 GPS-DEM over the glacier-free terrain to remove the vertical bias, and then applied this function to both the on- and off-glacier areas (Rolstad and others, 2009). The vertical accuracies (std dev.) of the DEMs ranged from ±0.11 to ±4.58 m (Table 1; Fig. S3).

Surface elevation changes and mass-balance calculations

We calculated the elevation differences for the 1981–2007, 2007–2009, 2009–2012 and 2012–2015 periods, with 2009–2012 and 2012–2015 differences based on the timing of the 2012 dGPS survey, which was conducted before the monsoon season (5–8 May 2012; Table 1). We further estimated the elevation changes for the 2007–2015 period to compare these results with those for the 2012–2015 period. We removed the outliers, which we defined as greater than ±3 NMAD from the mean elevation changes, from each 50 m band of the on-glacier area during the calculation periods. The elevation change uncertainty (σ_{dh}) was estimated based on the standard error, which employs a spatial autocorrelation and is described as follows (McNabb and others, 2019):

$$\sigma_{dh} = \sqrt{\frac{\sigma^2_{\text{stable}}}{n/(2L/r)} + \sigma^2_{\text{bias}}} \quad (1)$$

where σ_{stable} and n are the std dev. and number of pixels over the off-glacier area, respectively; L is the distance of the spatial autocorrelation (m); r is the pixel size and σ_{bias} is the mean elevation change over the off-glacier area. L is determined by the ranges of the spherical semivariogram models that were fitted to empirical variograms of the elevation differences over the off-glacier areas using a least-squares method (Rolstad and others, 2009; Wang and Kääb, 2015; Magnússon and others, 2016; Ragettli and others, 2016); this value varies between 173 and 1329 m for the five analysis periods (Fig. S4).

Finally, the area-weighted geodetic mass balances (B_g; m w.e.) were estimated as:

$$B_g = \left(\rho_i \frac{\sum_z dh_z \, A_z}{A_T} \right) / \rho_w \quad (2)$$

where dh_z (m) is the mean annual elevation change at a given 50 m elevation band, A_z and A_T (km^2) are the corresponding area of the mean elevation band between years t_1 and t_2 and the total area, respectively; ρ_i is the ice density (assumed to be 850 kg m^{-3}) and ρ_w is the water density (1000 kg m^{-3}; for unit conversion). We extrapolated dh_z above 5500 m (~9% of the total glacier area, as the GPS-DEMs were not constrained above this elevation) via linear regression, with dh_z set to zero if positive values were obtained (Sugiyama and others, 2013). The 1981 and 2015 hypsometries were obtained from the glacier areas and DEMs over the glacier. The HMA-DEM, which was corrected by the 2015 GPS-DEM (Fig. S3f), was used for the 2015 hypsometry calculation since the UAV-DEM covered only ~70% of the glacier area (Fig. 1d). Furthermore, we estimated the 2007, 2009 and 2012 hypsometries from the 1981 and 2015 DEMs by assuming that the hypsometry varies linearly over time (Wagnon and others, 2021), because DEMs that covered the entire glacier were not available for these three years. We therefore note that the delineated glacier areas in 2007, 2009 and 2012 were not used for the B_g calculations.

The uncertainties in the area-weighted geodetic mass balance (σ_g) were evaluated using the uncertainties in the elevation changes (σ_{dh_z}), glacier area delineation (σ_{A_z}) and density assumption ($\sigma_{\rho i}$) in each elevation band, which were based on the method of Tshering and Fujita (2016):

$$\sigma_g = \frac{\sum_z \rho_i A_z \sigma_{dh_z} + \sum_z \sigma_{A_z} |dh_z| + \sum_z \sigma_{\rho_i} A_z |dh_z|}{A_T \, \rho_w} \quad (3)$$

Here we used σ_{dh} as the elevation change uncertainty in each band (σ_{dh_z}). We applied the root mean square errors of the linear regression against the mean elevation changes in each elevation band as the uncertainty (~0.62 m a^{-1}) for the areas where the elevation changes were extrapolated (>5500 m elevation). The uncertainties in the glacier area were estimated from the glacier boundaries and the DEMs in 1981 and 2015, where we assumed σ_{A_z} to be half a pixel for the referenced images (5 m for the 1981 map and 7.5 m for 2015 Landsat 8 OLI) multiplied by the glacier outline perimeters of each elevation band. The uncertainty in the density assumption was assumed to be 60 kg m^{-3}.

Results and discussion

The mean annual elevation changes for the five analysed intervals during the 1981–2015 period are shown in Figure 2. A relatively higher degree of variability is observed in the 2007–2009 elevation differences of both the off- and on-glacier areas (Fig. 2 and

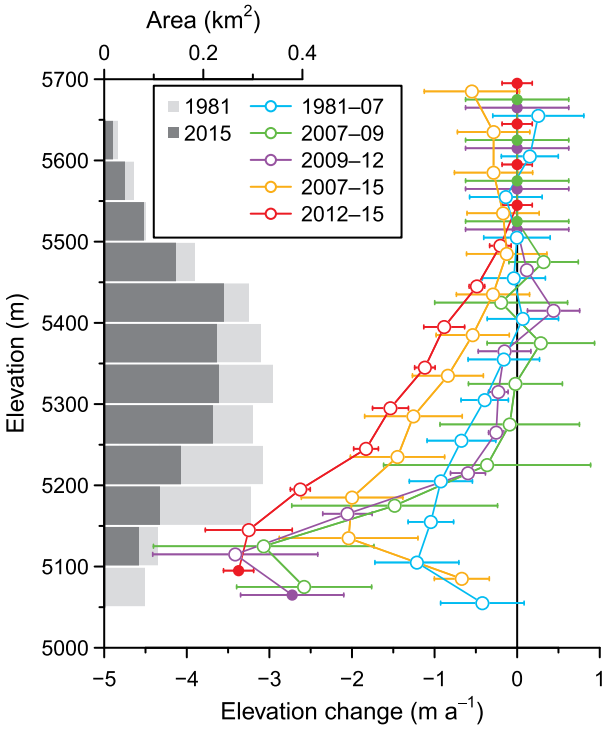

Fig. 2. Altitudinal distribution of the elevation changes (50 m averages) for the 1981–2007 (light blue), 2007–2009 (green), 2009–2012 (purple), 2007–2015 (orange) and 2012–2015 (red), with the1981 (grey) and 2015 (dark grey) hypsometries also shown. Error bars denote the std dev. of the elevation differences for a given elevation band. Filled circles with error bars denote the values where the elevation change was estimated via linear regression (assumed to be zero if the value is positive) and their associated uncertainties (root mean square errors).

https://doi.org/10.1017/jog.2022.118 Published online by Cambridge University Press

Table S3). The elevation differences for this interval are likely more affected than those for the other analysed periods, since the 2007 DEM was generated from only 14 oblique photographs and did not capture the glacier surface features as well as the 2009 DEM did. Furthermore, the short period of DEM coverage, in combination with the lower accuracy of the 2007 DEM, resulted in a relatively high σ_{dh} (0.24 m a^{-1}) for the 2007–2009 elevation change compared with those from the other periods (Table S3). Glacier thinning has been observed throughout the entire study period, with enhanced thinning in recent years. The maximum annual surface lowering is found around the lower bound of the glacier (~5200 m); large variations due to melting and retreating are also observed in this region (Fig. S5). The glacier boundaries (Fig. 1b and Table S4) and hypsometries (Fig. 2) also indicate continuous shrinkage from 2.42 km^2 in 1981 to 1.54 km^2 in 2015, with most of this shrinkage occurring around the lower bound of the glacier. Although elevation changes, which range from −0.92 to +0.44 m a^{-1}, have been observed along the central part of the glacier (5200–5500 m) during the 1981–2007, 2007–2009 and 2009–2012 periods, the accelerated surface lowering (~−1.83 m a^{-1}) was observed during the 2012–2015 and 2007–2015 periods. The spatial distribution of elevation changes for the two different periods (1981–2007 and 2007–2015) also revealed enhanced surface lowering from the terminus to the central part of the glacier (Fig. 3). Figure 4 depicts both the B_g calculations in this study, with −0.38 ± 0.16, −0.26 ± 0.30, −0.36 ± 0.17, −0.98 ± 0.27 and −0.74 ± 0.15 m w.e. a^{-1} for the 1981–2007, 2007–2009, 2009–2012, 2012–2015 and 2007–2015 periods, respectively, and the estimates from previous studies (Table 2).

Our results indicate that enhanced surface lowering has been propagating up-glacier in recent years (Fig. 2), with this trend likely due to the imbalance in recent climatic conditions, as indicated by previous studies (e.g. Sugiyama and others, 2013; Ragettli and others, 2016). Previous studies have revealed the annual precipitation at Kyangjin Village (~3900 m) has varied from 647 to 924 mm since 1988 (Racoviteanu and others, 2013; Shea and others, 2015). Shea and others (2015) estimated the elevation of the 0°C isotherm to be ~3000 and ~6000 m during the winter and monsoon seasons, respectively, which suggests that mostly liquid precipitation falls over the glacier during the monsoon season. Such a condition would heavily reduce the opportunity for glacier accumulation and thus cause the negative mass-balance, as indicated by Stumm and others (2021). Furthermore, Sugiyama and others (2013) attributed the surface flow velocity trend along the lower half of the glacier, where a drastic deceleration (60–90%) was observed during the 1981–2009 period, to ice thinning, which has also been confirmed for other Himalayan glaciers (Dehecq and others, 2019). A decrease in the flow velocity should reduce the ice flux, and therefore induce more surface lowering due to reduced compensation via the emergence velocity (e.g. Nuimura and others, 2011; Berthier and Vincent, 2012; Brun and others, 2018). These observations highlight the need to estimate and analyse the fluctuations in the long-term mass balance and emergence (submergence) velocity under recent climatic conditions, to evaluate the cause of this surface lowering in detail.

Many studies have quantified the area-weighted mass balance of Yala Glacier via in situ and/or remote-sensing approaches (Fig. 4 and Table 2). Ragettli and others (2016) reported B_g estimates of −0.28 ± 0.07 and −0.76 ± 0.24 m w.e. a^{-1} for the 1974–2006 and 2006–2015 periods, respectively. Fujita and Nuimura (2011) obtained B_g estimates of −0.68 and −0.80 m w.e. a^{-1}, each with a maximum uncertainty of 0.09 m w.e. a^{-1}, for the 1981–1996 and 1996–2009 periods, respectively, using much of the same data that were used in this study. Maurer and others (2019) estimated the elevation differences along glaciers

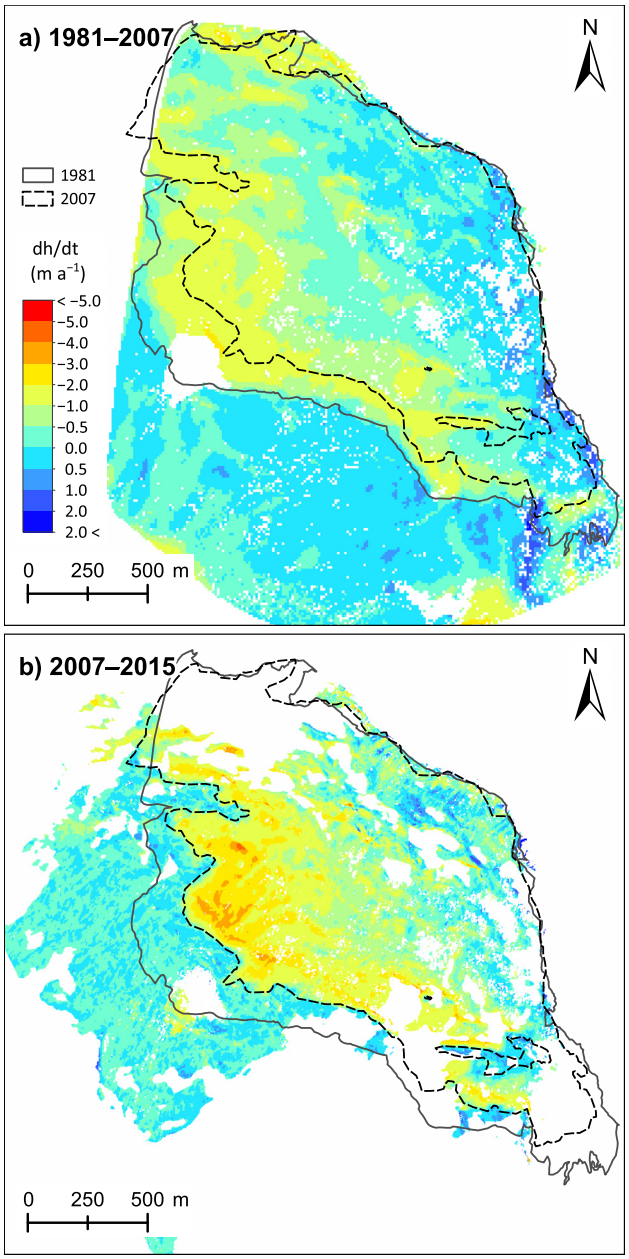

Fig. 3. Annual elevation changes across Yala Glacier for the (a) 1981–2007 and (b) 2007–2015 periods.

throughout the Himalaya via an analysis of declassified KH-9 Hexagon satellite and ASTER images (Fig. S6). We calculated B_g from the mean elevation difference profile (50 m bins) from Maurer and others (2019) using the hypsometries for the 1975–2000 and 2000–2016 periods, which were linearly estimated from the 1981 and 2015 hypsometries in this study, with B_g estimates of −0.28 ± 0.14 and −0.37 ± 0.20 m w.e. a^{-1} obtained for the 1975–2000 and 2000–2016 periods, respectively. Similarly, we estimated the B_g of Brun and others (2017) as −0.41 ± 0.23 m w.e. a^{-1} for the 2000–2016 period. A comparison of the B_g estimates from these previous studies indicates that our 1981–2007 B_g (−0.38 ± 0.16 m w.e. a^{-1}) is more negative than those by Ragettli and others (2016) and Maurer and others (2019) although it falls largely within the uncertainty ranges of these studies; however, the time periods are not exactly the same. In contrast, the estimated B_g for the 2007–2015 period (−0.74 ± 0.15 m w.e. a^{-1}) is consistent with those by Ragettli and others (2016), Shean and others (2020; −0.78 ± 0.13 m w.e. a^{-1} for the 2000–2018 period) and the direct measurement by Stumm and others (2021;

https://doi.org/10.1017/jog.2022.118 Published online by Cambridge University Press

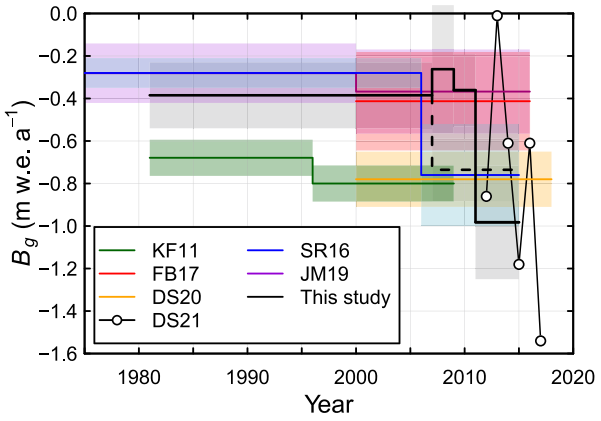

Fig. 4. Time series of the area-weighted glacier mass balances (B_g) for Yala Glacier estimated from this study (black line) and previous studies (KF11: Fujita and Nuimura, 2011; SR16: Ragettli and others, 2016; FB17: Brun and others, 2017; JM19: Maurer and others, 2019; DS20: Shean and others, 2020). Open circles and the dashed line indicate the in situ mass balance (DS21: Stumm and others, 2021). Shaded regions denote the uncertainties associated with each B_g calculation. Note that the B_g calculations from FB17 and JM19 were estimated using the mean elevation change profiles in FB17 and JM19 and the hypsometries from this study.

Table 2. Area-weighted glacier mass balance (B_g) for Yala Glacier that were derived in this and previous studies

Source	Period	B_g (m w.e. a^{-1})
This study	1981–2007/2007–2015	−0.38 ± 0.16/−0.74 ± 0.15
	2007–2009	−0.26 ± 0.30
	2009–2012	−0.36 ± 0.17
	2012–2015	−0.98 ± 0.27
Fujita and Nuimura (2011)	1981–1996/1996–2009	−0.68 ± 0.09/−0.80 ± 0.09
Ragettli and others (2016)	1974–2006/2006–2015	−0.28 ± 0.07/−0.76 ± 0.24
Brun and others (2017)	2000–2016	−0.41 ± 0.23
Maurer and others (2019)	1975–2000/2000–2016	−0.28 ± 0.14/−0.37 ± 0.20
Shean and others (2020)	2000–2018	−0.78 ± 0.13
Stumm and others (2021)	2011–2017	−0.80 ± 0.28

Note that the values from Maurer and others (2019) and Brun and others (2017) were calculated using the hypsometry in this study and the 50 m binned mean elevation changes from their respective studies.

−0.80 ± 0.28 m w.e. a^{-1} for the 2011–2017 period), whereas the estimate by Brun and others (2017) is less negative than these values. The difference among our 1981–2007 B_g and those of previous studies is likely due to the DEM accuracies, as the two DEMs, which are based on a 1981 map in this study and a KH-9 Hexagon image in the previous studies (Ragettli and others, 2016; Maurer and others, 2019), may contain errors. The 1981 map was derived from ground photogrammetry using base points that were horizontally 2 km from the glacier terminus, thereby suggesting a lower accuracy over the up-glacier part (~5600 m) of the glacier due to the relatively large distance between the base points and the snow-covered area. Furthermore, satellite-based DEMs generally possess larger uncertainties that are mainly present across the poorly contrasted snowfields (accumulation area). The trend in the surface elevation changes, with the exception of that in the terminus area (~5200 m), has even varied among these recent satellite-based studies (Fig. S6). Further research, including a comparison of the KH-9 DEM in previous studies and the GPS-DEM in this study, is therefore required to better understand the DEM accuracy and B_g differences before 2000. We also calculated an alternative B_g using the profiles in Fujita and Nuimura (2011) for the 1981–1996 period and the hypsometry employed in this study, which yielded a more plausible B_g estimate of −0.48 ± 0.14 m w.e. a^{-1}. This alternative calculation suggests the importance of employing a precise hypsometry for B_g estimations.

Our results reveal that Yala Glacier has undergone continuous mass loss since 1981, with an unabated acceleration in mass loss in recent years, which is in agreement with previous studies along this glacier (e.g. Sugiyama and others, 2013; Ragettli and others, 2016; Stumm and others, 2021) and/or the glaciers across the region (e.g. Maurer and others, 2019). Furthermore, the estimated B_g for the 2007–2015 period was more negative than both the regional mean geodetic mass balances for central Nepal (−0.46 ± 0.12 m w.e. a^{-1}) and debris-free glaciers in the Himalaya (−0.38 ± 0.08 m w.e. a^{-1}) during the 2000–2016 period (Maurer and others, 2019). Small debris-free glaciers that are located at relatively lower elevations in the Himalaya have exhibited similar large mass loss trends in recent years (e.g. Tshering and Fujita, 2016; Sherpa and others, 2017) and would therefore suffer from an acceleration in mass loss. Stumm and others (2021) also mentioned that low-lying glaciers with small elevation range tend to have more negative mass balances in terms of representativeness for the regional mass balance. Although mass-balance studies have been conducted across high-elevation glaciers (e.g. Sunako and others, 2019; Wagnon and others, 2021) and debris-covered glaciers (e.g. Dobhal and others, 2013; Vincent and others, 2016; Angchuk and others, 2021) using both glaciological and geodetic methods, studies that analyse smaller glaciers, such as Yala Glacier, are necessary to better understand the responses of these small glaciers to a warming climate.

Conclusions

We analysed and re-evaluated the surface elevation changes of Yala Glacier in the Nepal Himalaya using multiple datasets, which were derived from ground and aerial photogrammetry surveys, and dGPS measurements, for the 1981–2007, 2007–2009, 2009–2012, 2012–2015 and 2007–2015 periods. Significant surface lowering was observed ~5100–5200 m, with large variations due to glacier melt and retreat. The up-glacier propagation of this surface lowering trend has been enhanced in recent years (2012–2015 and 2007–2015) compared with the earlier periods. We further estimated the area-weighted glacier mass balance, which is −0.38 ± 0.16, −0.26 ± 0.30, −0.36 ± 0.17, −0.98 ± 0.27 and −0.74 ± 0.15 m w.e. a^{-1} for the 1981–2007, 2007–2009, 2009–2012, 2012–2015 and 2007–2015 periods, respectively. Although relatively large mass loss was estimated for the 1981–2007 period compared with those estimated in previous studies owing to the reduced accuracy of the DEM and/or different hypsometries, the results for the other time periods, especially the 2007–2015 (−0.74 ± 0.15 m w.e. a^{-1}) period, were mainly consistent with those estimated by the three previous studies (from −0.76 to −0.80 m w.e. a^{-1}) using different approaches, which indicate an acceleration in glacier mass loss in recent years. Such a rapid reduction in glacier volume, as has been observed for Yala Glacier, may affect the water supply to local communities, thereby warranting the need for continuous glacier measurements using both in situ and remote-sensing data to monitor future glacier fluctuations.

Supplementary material. The supplementary material for this article can be found at https://doi.org/10.1017/jog.2022.118.

Data. The DEMs and ortho images in 1981, 2007 and 2015 that were generated in this study are available online (https://doi.org/10.5281/zenodo.7412758). The GPS data are also available from the corresponding author upon reasonable request.

Acknowledgements. We are grateful to E. Berthier for providing the Pléiades satellite data. The Pléiades stereo pair used in this study was provided

by the Pléiades Glacier Observatory initiative of the French Space Agency (CNES). We wish to thank Asahi Shimbun Co., Ltd., for supporting the 2007 aerial photogrammetry survey. We express our thanks to Guide For All Seasons for their logistical support during the fieldwork and Prodrone Co., Ltd., for their dedicated UAV support. We are also indebted to all of the people who were involved in acquiring the observations during the fieldwork. Finally, we thank two anonymous reviewers and Scientific Editor J. M. Shea for their insightful comments and suggestions, which greatly improved the manuscript.

Authors' contributions. K. F. designed this study. S. S., K. F., T. I. and S. Y. conducted the field observations with the support of R. B. K. K. F. collected and analysed the GPS data. T. I. and S. S. conducted the UAV photogrammetry survey. S.S. analysed all of the DEMs. S. S., K. F. and A. S. wrote the manuscript with the help of S. Y. All of the authors equally contributed to the discussion.

References

Acharya A and Kayastha RB (2019) Mass and energy balance estimation of Yala Glacier (2011–2017), Langtang Valley, Nepal. *Water* **11**, 6. doi: 10.3390/w11010006

Ageta Y, Iida H and Watanabe O (1984) Glaciological studies on Yala Glacier in Langtang Himal. *Bulletin of Glaciological Research* **2**, 41–47.

Agisoft (2020) Agisoft Metashape User Manual, Professional Edition, Version 1.6, 154 pp.

Angchuk T and 7 others (2021) Annual and seasonal glaciological mass balance of Patsio Glacier, western Himalaya (India) from 2010 to 2017. *Journal of Glaciology* **67**, 1137–1146. doi: 10.1017/jog.2021.60

Azam MF and 10 others (2016) Meteorological conditions, seasonal and annual mass balances of Chhota Shigri Glacier, western Himalaya, India. *Annals of Glaciology* **57**(71), 328–338. doi: 10.3189/2016aog71a570

Azam MF and 5 others (2018) Review of the status and mass changes of Himalayan-Karakoram glaciers. *Journal of Glaciology* **64**(243), 61–74. doi: 10.1017/jog.2017.86

Berthier E and Vincent C (2012) Relative contribution of surface mass-balance and ice-flux changes to the accelerated thinning of Mer de Glace, French Alps, over 1979–2008. *Journal of Glaciology* **58**(209), 501–512. doi: 10.3189/2012JoG11J083

Berthier E and 10 others (2014) Glacier topography and elevation changes derived from Pléiades sub-meter stereo images. *The Cryosphere* **8**, 2275–2291. doi: 10.5194/tc-8-2275-2014

Brun F, Berthier E, Wagnon P, Kääb A and Treichler D (2017) A spatially resolved estimate of High Mountain Asia glacier mass balances from 2000 to 2016. *Nature Geoscience* **10**, 668–673. doi: 10.1038/ngeo2999

Brun F and 9 others (2018) Ice cliff contribution to the tongue-wide ablation of Changri Nup Glacier, Nepal, central Himalaya. *The Cryosphere* **12**, 3439–3457. doi: 10.5194/tc-12-3439-2018.

Dehecq A and 9 others (2019) Twenty-first century glacier slowdown driven by mass loss in High Mountain Asia. *Nature Geoscience* **12**, 22–27. doi: 10.1038/s41561-018-0271-9

Dobhal DP, Mehta M and Srivastava D (2013) Influence of debris cover on terminus retreat and mass changes of Chorabari Glacier, Garhwal region, central Himalaya, India. *Journal of Glaciology* **59**(217), 961–971. doi: 10.3189/2013JoG12J180

Fujita K and Nuimura T (2011) Spatially heterogeneous wastage of Himalayan glaciers. *Proceedings of the National Academy of Sciences* **108**, 14011–14014. doi: 10.1073/pnas.1106242108

Fujita K, Suzuki R, Nuimura T and Sakai A (2008) Performance of ASTER and SRTM DEMs, and their potential for assessing glacial lakes in the Lunana region, Bhutan Himalaya. *Journal of Glaciology* **54**(185), 220–228. doi: 10.3189/002214308784886162

Fujita K and 13 others (2017) Anomalous winter-snow-amplified earthquake-induced disaster of the 2015 Langtang avalanche in Nepal. *Natural Hazards and Earth System Sciences* **17**, 749–764. doi: 10.5194/nhess-17-749-2017

Höhle J and Höhle M (2009) Accuracy assessment of digital elevation models by means of robust statistical methods. *ISPRS Journal of Photogrammetry and Remote Sensing* **64**, 398–406. doi: 10.1016/j.isprsjprs.2009.02.003

Immerzeel WW and 6 others (2014) High-resolution monitoring of Himalayan glacier dynamics using unmanned aerial vehicles. *Remote Sensing of Environment* **150**, 93–103. doi: 10.1016/j.rse.2014.04.025

King O, Quincey DJ, Carrivick JL and Rowan AV (2017) Spatial variability in mass loss of glaciers in the Everest region, central Himalayas, between 2000 and 2015. *The Cryosphere* **11**(1), 407–426. doi: 10.5194/tc-11-407-2017

Kraaijenbrink PDA, Shea JM, Pellicciotti F, de Jong SM and Immerzeel WW (2016) Object-based analysis of unmanned aerial vehicle imagery to map and characterise surface features on a debris-covered glacier. *Remote Sensing of Environment* **186**, 581–595. doi: 10.1016/j.rse.2016.09.013

Lucieer A, Jong SMD and Turner D (2014) Mapping landslide displacements using Structure from Motion (SfM) and image correlation of multi-temporal UAV photography. *Progress in Physical Geography* **38**, 97–116. doi: 10.1177/0309133313515293

Magnússon E, Belart JMC, Pálsson F, Ágústsson H and Crochet P (2016) Geodetic mass balance record with rigorous uncertainty estimates deduced from aerial photographs and lidar data – case study from Drangajökull ice cap, NW Iceland. *The Cryosphere* **10**, 159–177. doi: 10.5194/tc-10-159-2016

Maurer JM, Schaefer JM, Rupper S and Corley A (2019) Acceleration of ice loss across the Himalayas over the past 40 years. *Science Advances* **5**, eaav7266. doi: 10.1126/sciadv.aav7266.

McNabb R, Nuth C, Kääb A and Girod L (2019) Sensitivity of glacier volume change estimation to DEM void interpolation. *The Cryosphere* **13**, 895–910. doi: 10.5194/tc-13-895-2019

Mishra NB, Miles ES, Chaudhuri G and Mainali KP (2021) Quantifying heterogeneous monsoonal melt on a debris-covered glacier in Nepal Himalaya using repeat uncrewed aerial system (UAS) photogrammetry. *Journal of Glaciology* **68**(268), 1–17. doi: 10.1017/jog.2021.96

Nuimura T, Fujita K, Yamaguchi S and Sharma RR (2012) Elevation changes of glaciers revealed by multitemporal digital elevation models calibrated by GPS survey in the Khumbu region, Nepal Himalaya, 1992–2008. *Journal of Glaciology* **58**(210), 648–656. doi: 10.3189/2012jog11j061

Nuimura T and 5 others (2011) Temporal changes in elevation of the debris-covered ablation area of Khumbu Glacier in the Nepal Himalaya since 1978. *Arctic, Antarctic, and Alpine Research* **43**, 246–255. doi: 10.1657/1938-4246-43.2.246

Racoviteanu AE, Armstrong R and Williams MW (2013) Evaluation of an ice ablation model to estimate the contribution of melting glacier ice to annual discharge in the Nepal Himalaya. *Water Resources Research* **49**, 5117–5133. doi: 10.1002/wrcr.20370

Ragettli S, Bolch T and Pellicciotti F (2016) Heterogeneous glacier thinning patterns over the last 40 years in Langtang Himal, Nepal. *The Cryosphere* **10**, 2075–2097. doi: 10.5194/tc-10-2075-2016

Rolstad C, Haug T and Denby B (2009) Spatially integrated geodetic glacier mass balance and its uncertainty based on geostatistical analysis: application to the western Svartisen ice cap, Norway. *Journal of Glaciology* **55**(192), 666–680. doi: 10.3189/002214309789470950

Sato Y and 8 others (2021) Ice cliff dynamics of debris-covered trakarding glacier in the Rolwaling Region, Nepal Himalaya. *Frontiers of Earth Science* **9**, 1–14. doi: 10.3389/feart.2021.623623

Shea JM and 5 others (2015) A comparative high-altitude meteorological analysis from three catchments in the Nepalese Himalaya. *International Journal of Water Resources Development* **31**, 174–200. doi: 10.1080/07900627.2015.1020417

Shean DE (2017) *High Mountain Asia 8-Meter DEM Along-Track Optical Imagery, Version 1*. Boulder, CO, USA: NASA National Snow and Ice Data Center Distributed Active Archive Center. doi: 10.5067/GSACB044M4PK (Accessed on 21 April 2020).

Shean DE and 5 others (2020) A systematic, regional assessment of high mountain Asia glacier mass balance. *Frontiers of Earth Science* **7**, 1–19. doi: 10.3389/feart.2019.00363

Sherpa SF and 8 others (2017) Contrasted surface mass balances of debris-free glaciers observed between the southern and the inner parts of the Everest region (2007–15). *Journal of Glaciology* **63**(240), 637–651. doi: 10.1017/jog.2017.30

Stumm D, Joshi SP, Gurung TR and Silwal G (2021) Mass balances of Yala and Rikha Samba glaciers, Nepal, from 2000 to 2017. *Earth System Science Data* **13**(8), 3791–3818. doi: 10.5194/essd-13-3791-2021

Sugiyama S, Fukui K, Fujita K, Tone K and Yamaguchi S (2013) Changes in ice thickness and flow velocity of Yala Glacier, Langtang Himal, Nepal, from 1982 to 2009. *Annals of Glaciology* **54**(64), 157–162. doi: 10.3189/2013AoG64A111

Sunako S, Fujita K, Sakai A and Kayastha RB (2019) Mass balance of Trambau Glacier, Rolwaling region, Nepal Himalaya: in-situ observations,

long-term reconstruction and mass-balance sensitivity. *Journal of Glaciology* **65**(252), 605–616. doi: 10.1017/jog.2019.37

Tshering P and Fujita K (2016) First in situ record of decadal glacier mass balance (2003–2014) from the Bhutan Himalaya. *Annals of Glaciology* **57**(71), 289–294. doi: 10.3189/2016aog71a036

Vijay S and Braun M (2016) Elevation change rates of glaciers in the Lahaul-Spiti (Western Himalaya, India) during 2000–2012 and 2012–2013. *Remote Sensing* **8**, 1–16. doi: 10.3390/rs8121038

Vincent C and 10 others (2016) Reduced melt on debris-covered glaciers: investigations from Changri Nup Glacier, Nepal. *The Cryosphere* **10**, 1845–1858. doi: 10.5194/tc-10-1845-2016

Wagnon P and 10 others (2021) Reanalysing the 2007–19 glaciological mass-balance series of Mera Glacier, Nepal, Central Himalaya, using geodetic mass balance. *Journal of Glaciology* **67**(261), 117–125. doi: 10.1017/jog.2020.88

Wang D and Kääb A (2015) Modeling glacier elevation change from DEM time series. *Remote Sensing* **7**, 10117–10142. doi: 10.3390/rs70810117

Yao T and 14 others (2012) Different glacier status with atmospheric circulations in Tibetan Plateau and surroundings. *Nature Climate Change* **2**, 663–667. doi: 10.1038/nclimate1580

Yokoyama K (1984) Ground photogrammetry of Yala Glacier, Langtang Himal, Nepal Himalaya. *Bulletin of Glaciological Research* **2**, 99–105.

https://doi.org/10.1017/jog.2022.118 Published online by Cambridge University Press

Supplementary material to "Up-glacier propagation of surface lowering of Yala Glacier, Langtang Valley, Nepal Himalaya"

Sojiro Sunako, Koji Fujita, Takeki Izumi, Satoru Yamaguchi, Akiko Sakai and Rijan B. Kayastha

Table S1. Summary of the satellite datasets used in this study.

Date (YYYYMMDD)	Sensor	Scene ID / dataset name	Resolution (m)	Role
19881012	Landsat 5 TM	LT51410401988286BKT00	30	Georectification for MAP-DEM
20091107	Landsat 5 TM	LT51410402009311KHC00	30	Glacier outlines
20121006	ASTER	ASTB121006050501	15	Glacier outlines
20151023	Landsat 8 OLI	LC81410402015296LGN01	15	Glacier outlines
20151229	World View-1	HMA_DEM8m_AT_20151229_0721_ 10200100496BE700_1020010046506C00	8	Hypsometry calculation
20171022	Pléiades	PGO_2017-10-22_Langtang	2 (DEM) 0.5 (ortho)	GCP collection

Table S2. Summary of the camera and SfM processing settings and generated DEM and ortho image details.

Information/Parameter setting	2007	2015
Camera and GCP		
Camera	Canon EOS 5D Canon EOS-1Ds Mark2	Sony a7R
Focal length (mm)	27–135	28
Number of Images	14	519
Image size (pixels)	4368 × 2912 (5D) 4992 × 3328 (1Ds Mark2)	6000 × 4000
GSD* (m)	1.38	0.05
Number of GCPs	32	5
SfM-MVS processing Parameter		
Alignment accuracy	Ultra high	High
Number of dense point clouds ($\times 10^5$)	87	1583
Quality for dense point clouds	Ultra high	High
Depth filtering	Moderate	Aggressive
Surface type	Arbitrary	Arbitrary
Face count ($\times 10^5$)	100	709
DEM/Ortho images		
Source	Mesh	Mesh
DEM/Ortho Resolution (m)	2.00/1.38	1.00/0.07
DEM size (pixels)	15667 × 16162	3436 × 3499
Ortho image size (pixels)	3800 × 4983	36270 × 35644

* Ground sampling distance.

Table S3. Number of points, mean (σ_{bias}), standard deviation (σ_{stable}) and uncertainty (σ_{dh}) of the elevation changes on the off-glacier area for each analysis period.

Analysis Period	Number of off-glacier points	σ_{bias} (m / m a^{-1})	σ_{stable} (m / m a^{-1})	σ_{dh} (m / m a^{-1})
1981–2007	7794	3.00 / 0.12	5.47 / 0.21	3.13 / 0.12
2007–2009	3459	−0.35 / −0.17	1.53 / 0.77	0.49 / 0.24
2009–2012	3215	0.01 / 0.00	0.15 / 0.07	0.10 / 0.05
2012–2015	864	0.08 / 0.02	0.41 / 0.10	0.53 / 0.13
2007–2015	199417	−0.34 / −0.04	1.41 / 0.18	0.35 / 0.04

Table S4. Summary of the glacier area estimated via manual delineation and linear estimation.

Year	Area (km^2)	
	Manual delineation	Linear estimation
1981	2.42	—
2007	1.91	1.74
2009	1.84	1.69
2012	1.66	1.61
2015	1.54	—

Fig. S1. Image of the hexacopter (PD6-NPL) used in this study. The greatest width is ~1.2 m.

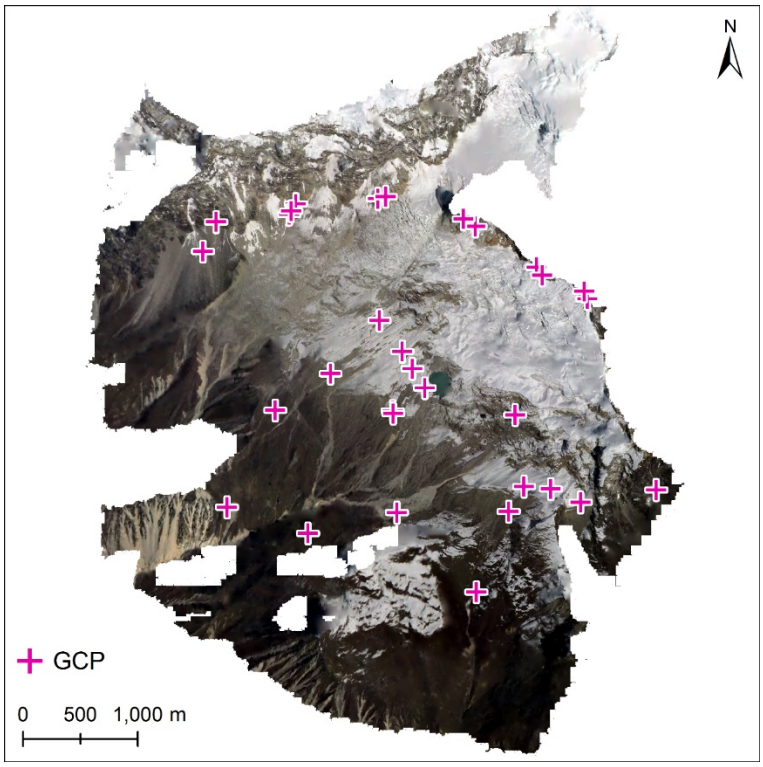

Fig. S2. GCP locations, which were derived from the Pléiades image, used to produce the 2007 DEM and ortho image.

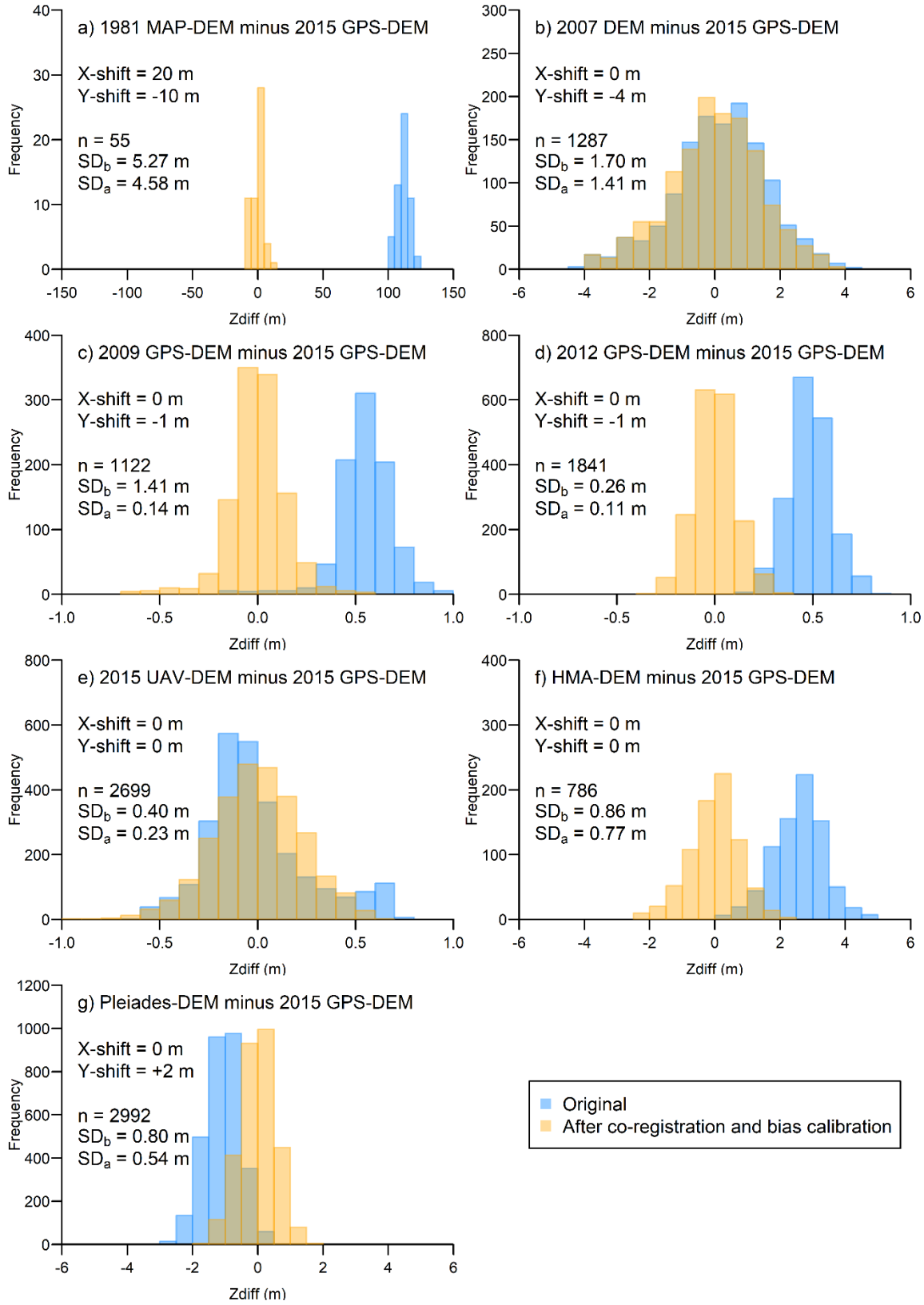

Fig. S3. Histograms of the elevation differences between the 2015 GPS-DEM and the other DEMs. SD_b and SD_a are the standard deviations of the elevation changes before and after co-registration and bias calibration, respectively.

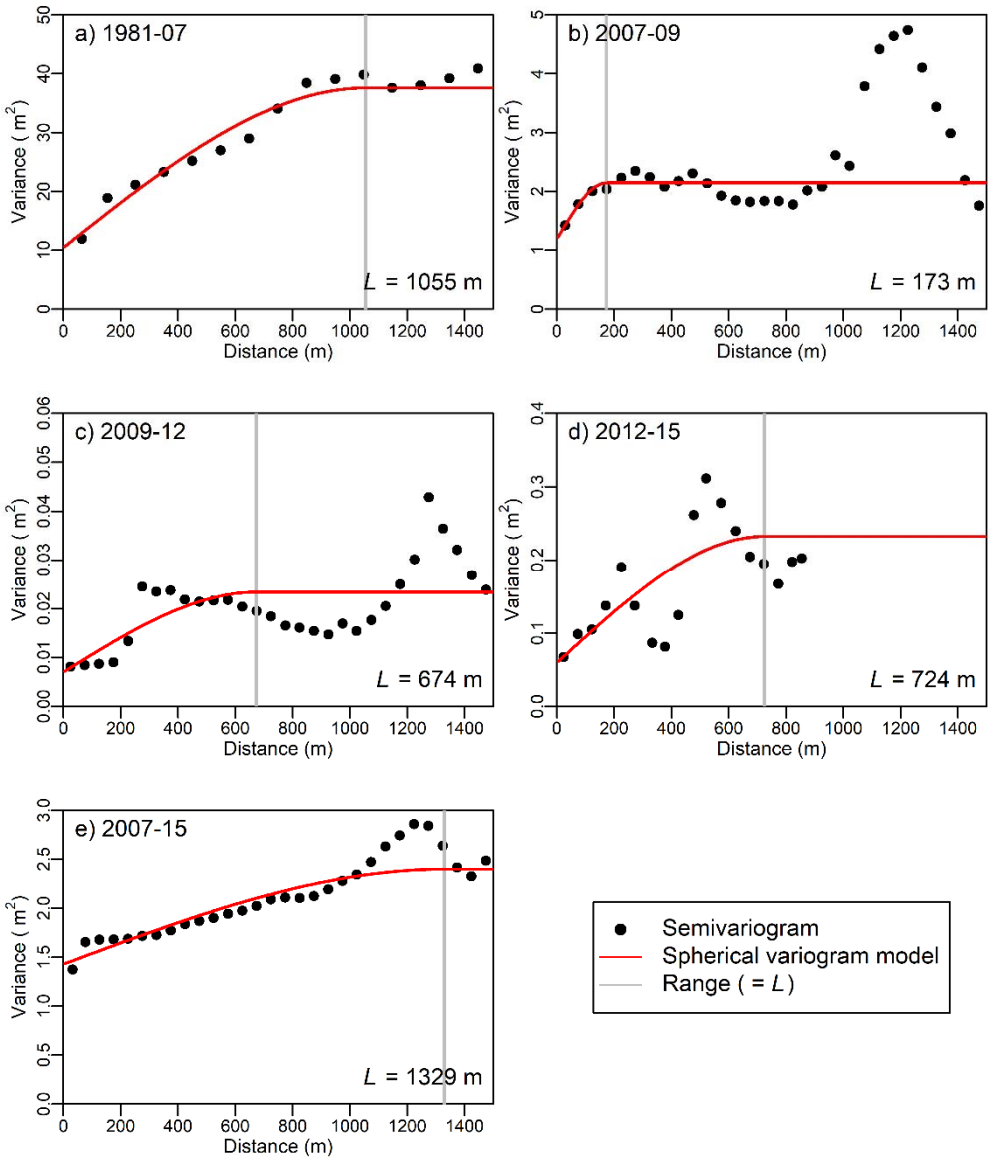

Fig. S4. Semivariograms of the elevation differences over the off-glacier areas for the five analysed intervals during the 1981–2015 period. Single spherical semivariogram models (red lines) are fitted to the empirical variograms (black dots). Grey lines show the range parameters (L). The empirical semivariograms are binned in 50 m intervals, with the exception of the 1981–2007 period, which is binned at 100 m interval to obtain a better fit and capture of the large scale trend.

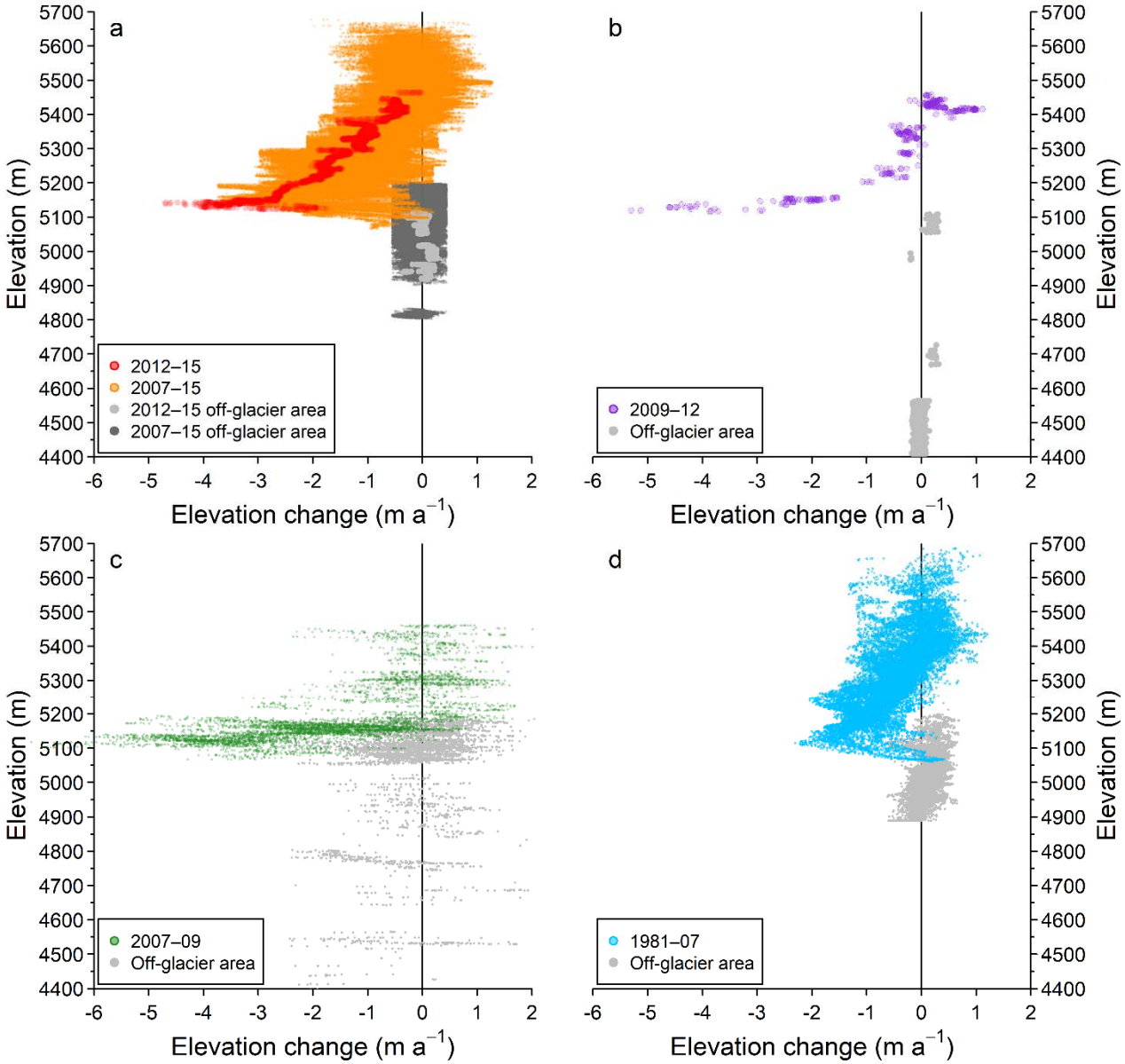

Fig. S5. Altitudinal distribution of the elevation changes for each calculation period (a–d). Grey dots in (a–d) and dark grey dots in (a) show the elevation change values for the off-glacier areas, respectively.

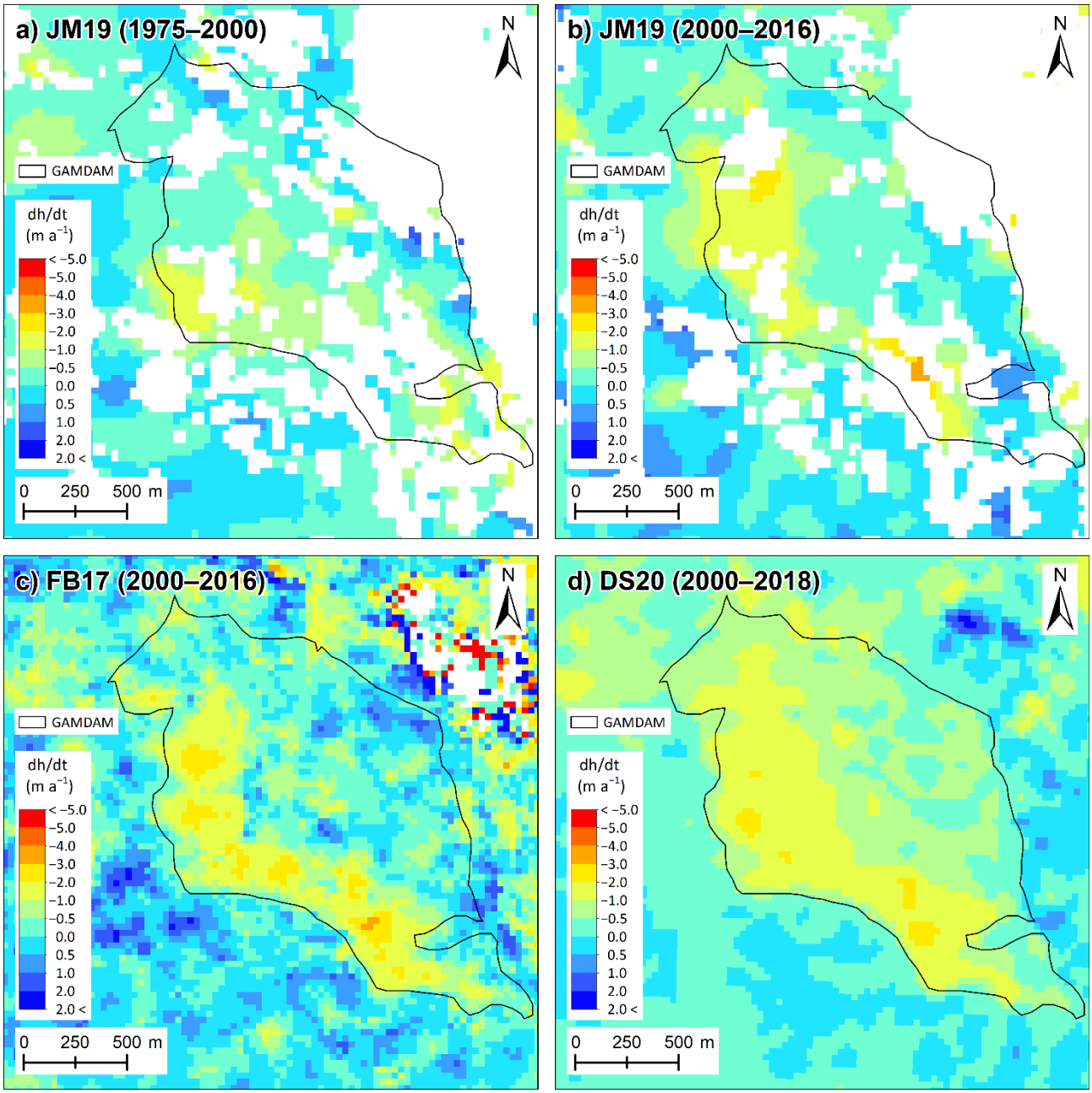

Fig. S6. Spatial distribution of the elevation changes across Yala Glacier that were derived from: a) and b) Maurer and others (2019), c) Brun and others (2017) and d) Shean and others (2020). The glacier polygon is taken from the GAMDAM Glacier Inventory (Sakai, 2019).

Reference

Sakai A (2019) Brief Communication: Updated GAMDAM Glacier Inventory over the High Mountain Asia. *The Cryosphere* **13**, 2043–2049 (doi:10.5194/tc-13-2043-2019)